Mon. Not. R. Astron. Soc. **000**, 1–14 (2013) Printed 22 June 2014 (MN LATEX style file v2.2)

Age and metallicity gradients support hierarchical formation for M87⋆

Mireia Montes[1,2]†, Ignacio Trujillo[1,2], M. Almudena Prieto[1,2] and José A. Acosta-Pulido[1,2]
[1] *Instituto de Astrofísica de Canarias (IAC), Vía Láctea s/n, La Laguna, E-38200, Spain*
[2] *Departamento de Astrofísica, Facultad de Física, Universidad de La Laguna, Astrofísico Fco. Sánchez s/n, La Laguna, E-38207, Spain*

arXiv:1401.1664v1 [astro-ph.GA] 8 Jan 2014

Accepted 2014 January 5. Received 2013 December 19; in original form 2013 August 7

ABSTRACT

In order to probe the inside-out formation of the most massive galaxies in the Universe, we have explored the radial ($0.1 \lesssim R \lesssim 8$ kpc) variation of the spectral energy distribution (SED) of M87 from UV to IR. For this purpose, we have combined high resolution data in 16 different bands. Our analysis indicate that the age of the stellar population of M87 remains almost unchanged with radius. However, the metallicity ([Z/H]) profile presents three different zones: the innermost kpc shows a *plateau* with supersolar metallicity, followed by a decline in metallicity down to 5 kpc and another *plateau* afterwards. The size of the inner *plateau* is similar to the expected size (R_e) of an object with the predicted mass of M87 at $z = 2$. The global [Z/H] gradient is -0.26 ± 0.10, similar to those found in other nearby massive ellipticals. The observed change in the stellar population of M87 is consistent with a rapid formation of the central part ($R \lesssim$ 5kpc) of this galaxy followed by the accretion of the outer regions through the infall of more metal-poor material.

Key words: galaxies :individual: M87 – techniques: high angular resolution – galaxies: photometry – galaxies: evolution – galaxies: formation

1 INTRODUCTION

Massive early-type galaxies are now widely believed to have been assembled hierarchically through repeated mergers which provide a relatively constant flow of accreted mass over a long time. The innermost regions of massive galaxies appear to have formed the majority of their stars at high redshift and on short timescales (e.g. Thomas et al. 2005) whereas their outer parts are likely assembled as a consequence of multiple major and minor merging (e.g. Trujillo, Ferreras & de La Rosa 2011). This two-phase formation picture (e.g. Naab, Johansson & Ostriker 2009) agrees with the observed size evolution of the massive galaxies. At $z \sim 1$ (2) massive early-type galaxies ($M_* \sim 10^{11} M_\odot$) were a factor of 2 (4) smaller than present-day equal mass objects, having an average effective radii of only ~ 1 kpc at $z \sim 2$ (e.g. Daddi et al. 2005; Trujillo et al. 2006; Buitrago et al. 2008).

The merger, star formation and chemical enrichment history of massive galaxies are imprinted in their kinematics and chemical abundances. Consequently, measurements of these quantities on today massive galaxies should constrain their evolution and formation. Different formation scenarios predict different chemical enrichments for the massive galaxies. For instance, the classical model of monolithic collapse predicts that the inflowing gas is chemically enriched by evolving stars and contributes with metal-rich fuel for star formation. This inflowing gas gives rise to high metallicities in the galaxy centre and to significant logarithmic metallicity gradients that can be steeper than -1.0 and correlate strongly with galaxy mass (Eggen, Lynden-Bell & Sandage 1962; Larson 1974; Carlberg 1984). However, revised monolithic models predict shallower metallicity gradients of -0.3 to -0.5 for a few massive galaxies (e.g. Chiosi & Carraro 2002; Pipino, D'Ercole & Matteucci 2008; Pipino et al. 2010; Merlin et al. 2012). On the other hand, a hierarchical formation scenario, with major mergers, is expected to dilute the metallicity gradient (Kobayashi 2004), reaching values of -0.2.

Many observational probes of stellar populations have

⋆ Based on European Southern Observatory (ESO) Very Large Telescope (VLT) programs 074.B-0404(A) and 076.B-0493(A) and observations made with the NASA/ESA *Hubble Space Telescope*, obtained from the Data Archive at the Space Telescope Science Institute, which is operated by AURA, Inc., under NASA contract NAS 5-26555

† E-mail: mireia.montes.quiles@gmail.com (MM)

been carried out for nearby early-type galaxies. Colours are one of the easiest observables for extragalactic systems. For instance, it has been known that the centres of low-resdhift ellipticals are redder that their outskirsts (e.g. Franx & Illingworth 1990; Peletier, Valentijn & Jameson 1990). These colour gradients are generally attributed to gradients in metallicity although a small contribution due to age gradients is expected (e.g. Spolaor et al. 2010). Works as Ogando et al. (2005), Spolaor et al. (2010), Kuntschner et al. (2010) and La Barbera et al. (2010) show that logarithmic metallicity gradients in early-type galaxies are about -0.2 to -0.3 dex. In addition, Sánchez-Blázquez, Gorgas & Cardiel (2006), Kuntschner et al. (2010) and Loubser & Sánchez-Blázquez (2012) found age gradients compatible with zero. However, evidences for a positive age gradient are also reported (e.g. Baes et al. 2007; La Barbera et al. 2010). There are a few but increasing number of studies exploring age and metallicity gradients in nearby massive galaxies up to several effective radii of radial distance (Coccato, Gerhard & Arnaboldi 2010; Tal & van Dokkum 2011; Roediger et al. 2011; Greene et al. 2012; La Barbera et al. 2012). These studies also agree on a metallicity decrease of the stellar populations of massive galaxies towards the outer regions as well as a non negligible contribution of younger stars (La Barbera et al. 2012). As an example, Coccato, Gerhard & Arnaboldi (2010) studied one of the brightest galaxies in the centre of the Coma Cluster, NGC 4889. They found evidences in its metallicity profile that points out to hierarchical formation. Two different gradients can be seen for $R \lesssim 1.2R_e$ and $R \gtrsim 1.2R_e$. Furthermore, the abundance of [α/Fe] remains flat down to $1.2R_e$ but decreases outwards. These evidences suggest that the outer parts of that galaxy were formed by accretion of low-mass systems, i.e. satellite galaxies.

In this paper, we concentrate our analysis on M87. M87 is an interesting target to explore the formation of massive galaxies. Located at the centre of the Virgo cluster, this object is probably one of the oldest massive galaxies in the Universe (Kuntschner et al. 2010). In this sense, its innermost region was most likely formed very early-on and consequently its stellar population should reflect the evolutionary path followed by this galaxy. Davies, Sadler & Peletier (1993) provide absorption-line strengths for the centre of this galaxy reaching as far as $50''$ ($\sim$ 4 kpc). They found a negative gradient in Mg_2 and a positive gradient in H_β. However, the detected emission in H_β could produce a dilution on this absorption line. As Mg_2 can be understood as a direct measurement of metallicity (e.g. Kuntschner et al. 2010), their results point out to a negative gradient in metallicity. Furthermore, Kuntschner et al. (2010), using SAURON data for the inner $100''$ ($\sim$ 8 kpc) of the galaxy, found no noticeable age gradient but a negative metallicity gradient. On the contrary, Liu et al. (2005) found a negative, but shallower gradient in metallicity and also a negative age gradient from $40''$ to $500''$. To sum up, all these evidences point out to a negative gradient in metallicity although the age gradient is much more difficult to determine.

In this work, we take a step forward and explore with unprecedent resolution ($\sim 0\farcs3$) the variation of the spectral energy distributions (SEDs) of M87 from 0.1 kpc to $\sim$ 8 kpc using 16 different bands from the UV to the IR. The large wavelength range provided is crucial to obtain accurate estimates of age and metallicity (Anders et al. 2004).

The vicinity of M87 and the high spatial resolution (HR) of the present work allow us to explore for the first time the substructure of the age and metallicity profiles. Well differentiated regions in the profiles could be an indication of different epochs of formation of this galaxy. Our paper will focus on this.

The structure of this paper is as follows. A description of the data and the photometry is presented in Section 2. In Section 3, the colour (Section 3.1), age and metallicity (Section 3.2) gradients are derived and discussed. We discuss our results in Section 4. Finally, a summary is presented in Section 5. The distance adopted for M87 is D=16.1 Mpc (Blakeslee et al. 2001, i.e., at the distance of the galaxy, $1'' = 78$ pc). The photometry is given in the AB system unless indicated otherwise.

2 DATA

2.1 High resolution data

The analysis conducted in this paper is based on multiwavelength coverage of the galaxy, the same as used in Montes et al. (2013, submitted) for the analysis of the globular cluster population of the central region of M87. A brief description of the data is presented here. Table 1 provides a description of the main characteristics of the dataset. The NIR data consist on HR images in the J and K_s bands acquired with the Very Large Telescope (VLT) using the Nasmyth Adaptive Optics System plus the Near-Infrared Imager and Spectrograh (NAOS + CONICA, NaCo, $0\farcs0271$/pixel). The inner half square arcminute of M87 was observed in J and in K_s. The bright nucleus was used as reference for the adaptive optics. The achieved resolution was $0\farcs27$ (J) and $0\farcs19$ (K_s) measured as the full width at half maximum (FWHM) of the most compact source in each image. The NaCo data reduction was performed using the ECLIPSE package provided by ESO. Photometric calibration of the images make use of standard stars taken along with the science frames. An image taken with NICMOS camera 2 using the filter F160W was also added from the *HST* archive. Its field of view (FOV) is smaller ($19\farcs2 \times 19\farcs2$), so the photometry provided by this filter is limited to R$< 10''$. This NIR dataset was complemented with *HST* archival data covering the UV-optical range. The spatial resolution achieved is $\sim 0\farcs15$ for the ACS and $\sim 0\farcs22$ for the WFPC2.

STIS far UV MAMA (F25SFR2) and near UV MAMA (F25QTZ) images of the central region of M87 were also extracted from the archive although the images only overlap with half of the NaCo J-band field of view. The spatial resolution is $0\farcs13$. The HST images were combined using MULTIDRIZZLE (Fruchter & Hook 2002) to achieve the nominal resolution of each camera. MULTIDRIZZLE combines the aligned individual exposures, rejects outliers and removes the geometric distortions.

Filter	λ	$\Delta\lambda\,(\AA)$	Instrument	Pixel scale ($''/pixel$)	Exp. Time (s)	Date	Program
F25SRF2							
FUV-MAMA	1456.6	120.8	STIS@*HST*	0.025	3526	17/05/1999	8140
F25SRF2							
FUV-MAMA	1456.6	120.8	STIS@*HST*	0.025	2680	14/02/2002	8643
F25QTZ							
NUV-MAMA	2355.3	419.8	STIS@*HST*	0.025	2372	17/05/1999	8140
F336W	3359.5	204.5	WFPC2@*HST*	0.046/0.1	28800	25/12/2000	8587
F410M	4092.7	93.8	WFPC2@*HST*	0.046/0.1	19200	07/02/2001	8587
F467M	4670.2	75.3	WFPC2@*HST*	0.046/0.1	7200	28/12/2000	8587
F475W	4745.3	420.1	ACS/WFC@*HST*	0.05	750	19/01/2003	9401
F547M	5483.9	205.5	WFPC2@*HST*	0.046/0.1	7200	10/02/2001	8587
F555W	5442.9	522.2	WFPC2@*HST*	0.046/0.1	2430	03/02/1995	5477
F606W	5919.4	672.3	ACS/WFC@*HST*	0.05	28500	24/12/2005	10543
F658N	6590.8	29.4	WFPC2@*HST*	0.046/0.1	13900	09/05/1996	6296
F702W	6917.1	586.7	WFPC2@*HST*	0.046/0.1	280	23/01/1995	5476
F814W	8059.9	653.0	ACS/WFC@*HST*	0.05	72000	24/15/2005	10543
F850LP	9036.4	527.2	ACS/WFC@*HST*	0.05	1120	19/01/2003	9401
J	12650.0	2500.0	NACO@VLT	0.027	784	23/01/2006	$076.B-0493(A)$
F160W	16506.0	1177.3	NICMOS2@*HST*	0.075	32	20/11/1997	7171
K_s	21800.0	3500.0	NACO@VLT	0.027	300	23/01/2006	$076.B-0493(A)$

Table 1. Set of filters used in this study of M87 with HR.

2.2 Photometric profiles

2.2.1 High resolution profiles of the centre of M87

The HR surface brightness profiles of the centre of M87 in all filters were obtained using a custom-made task developed in IDL. The active nucleus and jet of M87 were identified and masked by eye while the detection of the globular clusters was made using SExtractor (Bertin & Arnouts 1996) and they were also masked. The central region of M87 is circular symmetric (Cohen 1986), so the photometry was extracted using circular annuli at different radial distances. To unify the effects of the resolution in the different images, we take 3 times the FWHM of the worst spatially resolved image (J) as the width of the rings for the photometry, i.e. $\sim 1''$. To avoid contamination due to the Point Spread Function (PSF) wings of the nuclear point source, the inner $1''$ was masked in all images. For each annulus, the surface brightness was obtained averaging the pixel values.

The prominent jet of M87 may have effects in the profiles of the galaxy. To test this possible source of contamination, we derived the surface brightness profiles at both sides around the nucleus: the right side, from the nucleus to the west, and the left side, from the nucleus to the east. The profiles of the right and left sides present the same properties within errors and the symmetry of the integrated properties of the galaxy are not affected by the presence of the extended component associated to the jet.

Our HR photometry is given in Table A1 and the profiles presented in Figure 1.

2.2.2 Wide-field profiles

To explore the stellar populations down to M87's effective radii ($R_e = 106\farcs2$, Falcón-Barroso et al. 2011), the HR data described above was complemented with 2MASS[1] (Jarrett et al. 2003), SDSS *griz* (Chen et al. 2010) and GALEX (Gil de Paz et al. 2007) surface brightness profiles collected from the literature. Typical spatial resolutions are: $\sim 3''$ for 2MASS (Skrutskie et al. 2006), $\sim 1\farcs5$ for SDSS (York et al. 2000), $\sim 4\farcs5$–$5''$ for GALEX (Gil de Paz et al. 2007). The exposure times of the images are: 7.8s for 2MASS, 55s for SDSS and 1585s for GALEX. In addition, we have downloaded the u band image from the SDSS archive to complement the profiles provided by Chen et al. (2010).

We also present a brief description of the derivation of the surface brightness profiles of this wide-field dataset. This is important to ensure that these profiles are consistent with our HR profiles. The 2MASS profiles (Jarrett et al. 2003) were derived using an almost circular annulus of axis ratio of 0.99. Likewise, the GALEX mean surface brightness were derived within elliptical ($\epsilon = 0.2$) annuli, as described in Gil de Paz et al. (2007). Chen et al. (2010) used the IRAF task ELLIPSE to derive the SDSS *griz* profiles, with variable ellipticity reaching a maximun of 0.13 for R$\sim R_e$, while for u we used circular annuli. The ellipticity values used to derive these profiles are very close to the circular apertures we used for the inner regions except in the case of the GALEX photometry. In any case, GALEX data will no be used to derive the main conclusions of this work as we will explain later on. The global extension of the radial profiles from the literature are: $240''$, $403''$ and $331''$, respectively. These profiles were used only up to $\sim 100''$ for reasons explained in the following sections. SDSS and GALEX photometry were kindly provided by the authors.

2.2.3 HR vs. wide-field photometry

The HR photometry, in Section 2.2.1, describe the very centre of the galaxy (R$<$ 1 kpc). The field of view of the cameras used to explore the inner region of M87 is entirely dominated by the flux of the galaxy as it is observing its inner regions. This results in an impossibility to obtain a proper sky background for these images. Therefore, the outer shape of the surface brightness profiles of the HR is compromised. To surpass this problem, we made use of wide field photome-

[1] http://irsa.ipac.caltech.edu/cgi-bin/2MASS/LGA/nph-lga?objstr=m87

try from the literature to determine down to which distance the radial profiles of the HR images are reliable. This is illustrated in Figure 1, where the surface brightness profiles are shown. The HR profiles are plotted down to the radial distances where they are reliable. Filled circles correspond to HR photometry while open circles depict wide-field profiles from the literature. These profiles indicate which filter was used at a certain radius. To show the agreement of the HR and the outer region photometry, the profiles shown in Figure 1 are shifted vertically for visualization purposes. As seen in Figure 1 the HR profiles in the optical bands reach down to 10″. For STIS F25QTZ, the distance reduces to 5.″5. Outwards, GALEX, SSDS and 2MASS photometry were used down to M87's R_e.

To avoid zeropoint biases among the different data, we decided to rely our analysis on the ground-based photometry and shift the HST profiles. In order to estimate the offsets between HR and wide-field profiles, we have compared the profiles at $\sim 10''$, to minimize the contribution of the PSF of the ground-based telescopes and the sky background oversubstraction in the HST bands. The offsets were calculated as the difference between the HST filters and the corresponding (or the nearest) ground-based filter. We provided the offsets and the root mean square (r.m.s) between HR and wide-field profiles in a common overlapping region (from 5″ to 10″) in Table B1 in Appendix B. In this overlapping region, the HR and wide-field data were used cojointly to build and analyse the SEDs, i.e. when estimating the $\tilde{\chi}^2$. This common HR and wide-field region is depicted by the superposition of open circles to the (smaller) filled, see Figure 1.

The photometry was corrected for Galactic reddening using the maps of Schlegel, Finkbeiner & Davis (1998) ($E(B-V) = 0.022$) and the Cardelli, Clayton & Mathis (1989) extinction law. The presence of almost no internal dust in this galaxy, as shown in Baes et al. (2010), indicates that internal dust extinction should not affect the results presented here.

2.2.4 Photometric uncertainty estimation

Obtaining a realistic error estimate of our photometry is crucial in order to constrain properly the age and metallicity of the stellar populations. As mentioned before, in the innermost region of M87 we have derived the photometric profiles using circular annuli at different radial distances and averaging the fluxes within the annuli. The nominal photometric uncertainty obtained in such way is extremely low (< 0.0003 mag) and does not reflect the real precision that can be expected. The two main sources of error are: the uncertainty in the photometric zeropoint and the photometrical uncertainties. Consequently, to get a much better estimation of the photometric errors, for each band we have fitted the radial profiles with a (Sérsic 1968) fit to determine the r.m.s of our profile data points in relation to the Sérsic fit. The Sérsic function is a three parameter law that is known to model very accurately the surface brightness profile of elliptical galaxies. For instance, it is known that the surface brightness profile of M87 was reported to follow a $R^{1/4}$ law (de Vaucouleurs & Nieto 1978). Hence, we have fitted the Sérsic model to our data and estimated its scatter around

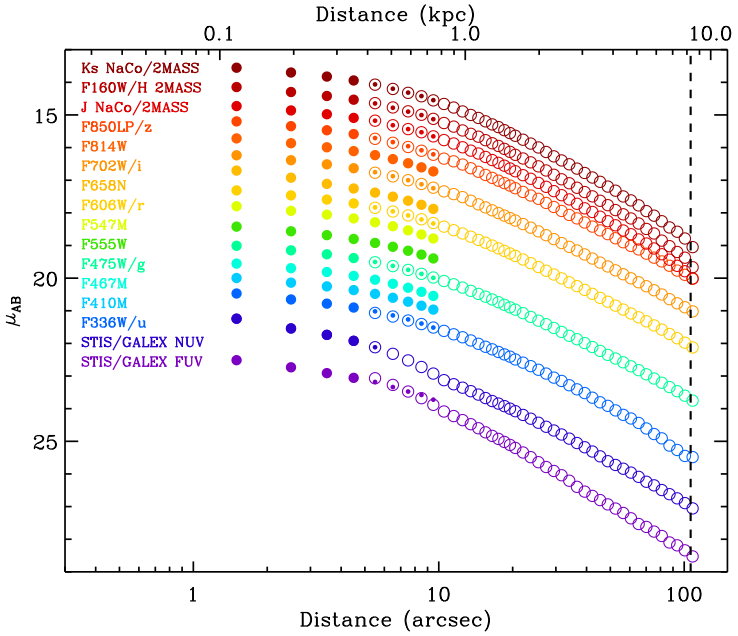

Figure 1. Surface brightness profiles of the multiwavelength dataset for M87 up to R_e. The vertical dashed line marks the position of the R_e. Different vertical shifts to the profiles were applied for visualization. Filled circles correspond to HR photometry while open circles depict wide-field profiles from the literature.

the fit for each band[2]. This scatter or deviation of the Sérsic profile should be a good indication of the real photometric error in each band. The residuals to the Sérsic fits are shown in Appendix B1. Therefore, the total errors, a combination of both zeropoint error and the photometric oscillation, are given in Table 2.

For consistency, we also estimate the photometric errors for the wide-field data using the same technique. It is worth noting that for 2MASS, the nominal errors are bigger than our estimates. Therefore, to be conservative, we used the nominal errors provided by 2MASS photometry.

In the following sections, the properties of the stellar populations of the central region of M87 are analysed in two ways. First, we explore the colour gradients, focusing in the new NIR imaging. Second, we fit the SEDs using SSPs models to derive the age and metallicity of the galaxy.

3 THE INNER ~ 8 KPC OF M87

We recall that the aim of this paper is to characterize the stellar population of the inner 8 kpc of M87 using unprecedent HR SED data for its most inner regions from UV to IR. Accesing a large wavelength range yields to more reliable estimates of age and metallicity, even for older ages

[2] It is worth noting that our intention with these Sérsic fitting is not obtaining an estimation of the structural parameters of M87 in different bands. The spatial range of our observations will not allow us to do that properly. Our goal is to have an independent photometric way of measuring the level of oscillation of our photometric data in relation to a smooth surface brightness distribution.

F25SFR2	F25QTZ	F336W	F410M	F467M	F475W	F555W	F547M
[mag/arcsec^2]							
0.054	0.299	0.033	0.026	0.030	0.026	0.025	0.039
F606W	F658N	F702W	F814W	F850LP	J	F160W	K_s
[mag/arcsec^2]							
0.025	0.051	0.026	0.026	0.026	0.045	0.052	0.059
FUV GALEX		NUV GALEX		u		g	
[mag/arcsec^2]							
0.107		0.103		0.029		0.013	
r	i	z	J	H	K_s		
[mag/arcsec^2]							
0.013	0.014	0.018	0.026*	0.031*	0.027*		

Table 2. Estimated photometric errors in each band. The errors in J, H and K_s (marked with asterisks) are smaller than the nominal errors provided by the 2MASS photometry. In those cases, we used the most conservative values provided by 2MASS.

(Anders et al. 2004). A first inspection of the radial profiles in all bands shows a smooth behaviour. Consequently, no drastic changes are expected in the stellar population properties but a mild increase or decrease variation. We have checked visually that the presence of a disk (R$\sim 1''$) and extended filaments (reaching $\sim 10''$) of ionized gas in the Hα + N[II] (F658N) image (Ford et al. 1994; Pogge et al. 2000) do not modify the profiles of the adjacent bands, e.g. F606W, F702W (see Figure 1).

3.1 Colour gradients

Radial colour gradients can provide valuable constraints in the formation processes of ellipticals. While the NIR wavelength range depends mainly on the red giant-branch, the optical regime depends on stars near the main sequence turn-off point being both metallicity and age sensitive. By using the combination of optical-IR colours, we have therefore a better chance to break the age-metallicity degeneracy inherent in optical colours alone (e.g. Kissler-Patig, Brodie & Minniti 2002). Optical-IR colours together with optical colours can separate the effects of metallicity and age (e.g. Peletier, Valentijn & Jameson 1990).

The four panels in Figure 2 show IR, optical and combinations of optical-IR and UV-optical colours. $r-K_s$, $g-z$ and $FUV-g$ correspond to $F606W-K_s$, $F475W-F850LP$ and $F25SFR2-F475W$ for the HST imaging of the central parts of the galaxy. The ACS filter F475W (F850LP) is analogous to SDSS g (z), so the comparison with the outer region of the galaxy is straightforward. A vertical shift to the $r-K_s$, $FUV-g$ and $J-K_s$ has to be applied to account for the difference among the filters: F606W and r, NaCo J and 2MASS J and STIS F25SFR2 and GALEX FUV. We have overplotted the data from Peletier (1989) for comparison. The observed colours agree with a mild decrease on the properties of the stellar population of the galaxy down to R_e. The decrement observed in all the colour profiles, except the UV colour, is in agreement with the broadband optical and NIR colours seen in Peletier (1989), although in 2MASS $J-K_s$ (purple triangles) the decrease seems less pronounced in our data. Regarding the UV colour, the FUV depends mainly on hot HB stars while the optical is dominated by main sequence and giant stars (Dorman, O'Connell & Rood 1995). Thus, $FUV-g$ is a measure of the UV excess and,

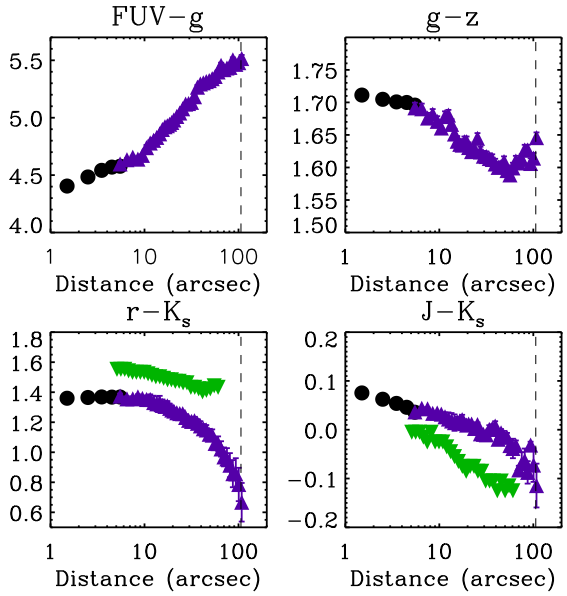

Figure 2. Radial UV-optical, optical, optical-IR and IR colours. Black dots refer to HR photometry. Purple triangles are SDSS+2MASS photometry and green inverted triangles correspond to the radial profiles of M87 from Peletier (1989). The vertical dashed line marks the position of the R_e. Peletier (1989) $J-K_s$ is shifted -0.05 mag for visualization.

consequently, of the fraction of the stellar population that appears in the form of hot HB stars. It is seen that $FUV-g$ is bluer in the central parts of the galaxy, thus the UV excess is more intense, as expected in Dorman, O'Connell & Rood (1995), and then becomes more and more faint with radius. Ohl et al. (1998) found that the $FUV-B$ colour profile is flat out to $20''$ and then the colour becomes redder with increasing radial distance. The contribution of the nucleus and jet is ruled out, as they only contribute about 17% of the light within $20''$. This result is in agreement with our $FUV-g$ colour.

In the inner $\sim 10''$ ($\lesssim 1$ kpc) the colour profiles present an almost flat slope compared to the wide-field imaging, except in the case of $J-K_s$, and only at larger distances the colours begin to drop. Further evidences of flat IR colour profiles in the inner regions of M87 down to $5''$ are found in Corbin, O'Neil & Rieke (2002). It is worth noting that

the $g-z$ colour shows an abrupt increase with radius for R$>50''$ not observed in any other colours in Figure 2, probably due to an incorrect sky background estimation or PSF issues (e.g. Tal & van Dokkum 2011). This is also observed in the $g-r$ colour. Regarding $J-K_s$, the higher errors and dispersion are produced by the low exposure times of 2MASS data. To estimate at which radius the 2MASS photometry is realiable, we have compared our K_s-band profile with the deeper K-band profile kindly provided by R. Läsker (priv. comm., Läsker, Ferrarese & van de Ven 2013). This comparison shows that both profiles are compatible in the central parts but at distances farther than $50''$ the 2MASS K_s profile becomes clearly underestimated. The increase in $g-z$ and the departure of the shape of 2MASS profiles beyond M87's R_e forced us to set the limit of our analysis to $\sim 100''$. In any case, the conclusions of this work do not rely in our observations for R$>50''$ (at those distances, we have used other data from the literature).

The colour gradients seem to correlate well among them. This indicates that both optical and optical-IR radial colour gradients are likely caused by an identical physical process. As the optical-IR traces metallicity, we can therefore expect that changes in these colours indicate changes in metallicity. Consequently, the metallicity gradient is very likely the main cause for the colour gradients in the other bands as well. On the following sections we expand on this possibility.

3.2 Age and metallicity gradients

Taking advantage on the large wavelength range of our dataset, we fitted single stellar population (SSP) models to explore whether it is possible to detect stellar population gradients in the inner 8 kpc of M87. SSP models are the most simple description we can make of our data. Note that this could be a rough assumption at large radii because we are considering a two-phase formation scenario (see the Introduction) and at large radii we expect the accretion of a variety of low-mass galaxies. We use the same approach as in Montes et al. (2013, submitted) to determine age and metallicity of the inner 3 square kpc M87 globular cluster population. We describe our approach in the following subsections.

3.2.1 Methodology

A SSP is defined as a single generation of coeval stars characterized by the same parameters, the most relevant being the metallicity, age and initial mass function (IMF). The observed SEDs are compared with some model SSPs to obtain information of the stellar populations of M87. Since our data are integrated luminosities, we convolved the theoretical SED spectra with the filter response of our photometric filters to retrieve synthetic photometry for comparison. The computed magnitude, in the AB system, for the i^{th} filter is

$$m^i_{AB} = -2.5 \log \frac{\int_\nu F_\nu \phi^i(\nu) d\nu}{\int_\nu \phi^i(\nu) d\nu} + 8.906, \quad (1)$$

where F_ν is the theoretical SSP SED expressed in Jy, which is a function of metallicity, age and luminosity, and ϕ^i is the response curve of the i^{th} filter. Given the wide wavelength coverage of M87 to find the most suitable SSP model, a reduced-χ^2 minimization approach is applied.

$$\tilde{\chi}^2 = \frac{1}{N-n-1} \sum_{i=1}^{15} \frac{(m_{obs,i} - m_{mod,i})^2}{\sigma_i^2}, \quad (2)$$

where $m_{mod,i}$ depend on age, metallicity and luminosity, N is the number of photometric filters, n is the number of fitted parameters and σ_i are the observational errors in the photometry of each band. As the parameters to fit are 3: age, metallicity and luminosity, the number of spectral bands required for the fit are at least 5.

To illustrate the reliability of our age and metallicity estimations, we followed the standard procedure to estimate the 68% and 95% confidence regions. For each solution we have calculated the value of the $\tilde{\chi}^2$ for each of our models (given by Equation 2). After finding the minimum and taking into account the degrees of freedom $(N-n-1)$, we have searched for all the solutions in the age and metallicity maps which are at a given distance of the minimum $\tilde{\chi}^2$ reduced value, corresponding to the 68% and 95% of probability as given by a chi-squared distribution table. The areas dictated by these limits represent our confidence interval solutions. Note that the degrees of freedom $(N-n-1)$ vary with radius.

The models used here are Bruzual & Charlot (2003, hereafter BC03) models. The BC03 SSP models contain 221 spectra describing the spectral evolution of SSPs from 0.1 Myr to 20 Gyr for 6 different metallicities: Z=0.0001, 0.0004, 0.004, 0.008, 0.02 ($Z_\odot$), 0.05 for two possible IMFs, Chabrier (Chabrier 2003) and Salpeter (Salpeter 1955). These models cover a range of wavelengths from 91 Å to 160 μm. As the age-metallicity grid is irregular, the metallicity vector was rebinned. The grid was expanded with 200 metallicities linearly interpolating the original SSPs. The maximum age of the BC03 is 20 Gyr, in excess with the current estimate of the age of the universe 13.8 Gyr (for a flat universe with $H_0 = 67.3$ km/s/Mpc, $\Omega_M = 0.315$, $\Omega_\Lambda = 0.685$, Planck Collaboration et al. 2013). Therefore, we restrict the available ages of the models to the maximum age of ~ 14 Gyr. We use the Salpeter IMF unless indicated otherwise. BC03 models provide Chabrier and Salpeter IMFs, but using a Salpeter IMF seems a reasonable choice taking into account the recent studies favouring this kind of IMF for the most massive galaxies in the universe (e.g. Cenarro et al. 2003; van Dokkum & Conroy 2010; Ferreras et al. 2013). The treatment of the TP-AGB stars in the new models (Charlot & Bruzual 2007, priv. comm.) tend to overestimate the contribution of these stars in the NIR (e.g. Zibetti et al. 2013). Nevertheless, we have confirmed that the same results presented below are obtained using the Charlot & Bruzual (2007, priv. comm.) models. This is discussed in more detail in Appendix C.

M87 is known to have a UV upturn for both globular clusters (Sohn et al. 2006) and the galaxy itself (Gil de Paz et al. 2007). This UV upturn is thought to be consequence of the presence of low-mass helium-burning stars, the so-called extreme horizontal branch (O'Connell 1999). The SSPs of BC03 do not include these hot horizontal branch stars, therefore it is not expected an agreement of the models with the observations in this particular wave-

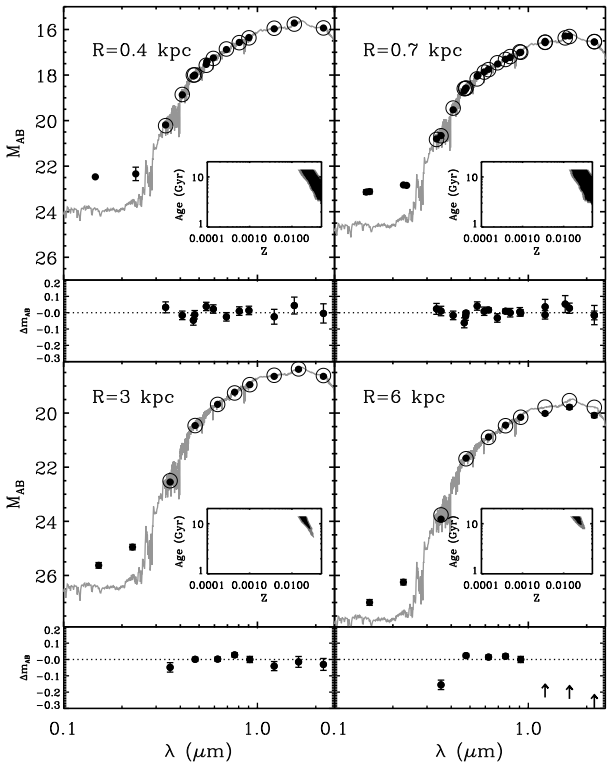

Figure 3. SEDs at four different radii (black dots) and the best fitting BC03 models (grey lines). The inset represents the age-metallicity parameter space and the contours of the 68% (black), and the 95% (grey). Note the age-metallicity degeneracy. The open circles represent the convolution model with the filter response in each bandpass. At large radii, the 2MASS IR data is underestimated due to incorrect background estimation. In the lower panels, the residuals between the model and observation are shown for each SED. For R$\sim$ 6 kpc, the lower limits in the IR photometry show the effect of the oversubstraction of the sky.

length range. For this reason, we exclude the UV data points from our fits.

In Figure 3, the best model fits are shown for 4 SEDs at different radial distances: 0.5 kpc, 1 kpc (R_e/8), 4 kpc and 8 kpc (R_e). The insets show the contours of the 68% and the 95% of probability. We can see the shift of the contours towards low metallicity as radial distance increases. For the fit at R$\sim$ 6 kpc, it is seen the effect of the underestimation of the u and 2MASS bands (lower limits).

3.2.2 Age and metallicity radial profiles

In Figure 4, the age and metallicity radial profiles of M87 obtained by fitting the models are shown. The grey polygon represent the 68% confidence region obtained from the fits to the radial SEDs (see Section 3.2.1). To illustrate the quality of the fits over the radial range, we show the minimum $\tilde{\chi}^2$ as a function of radius in Figure C1 in Appendix C. In Figure 4, we have overplotted other data obtained from the literature. Purple stars are data from Davies, Sadler & Peletier (1993) from absorption-line strength of Mg_2 transformed to Z using the relationship provided in Casuso et al. (1996). Red squares represent the data obtained with SAURON for the central region of M87 (Kuntschner et al. 2010). The red square in the age (left plot) represents the age profile derived from the SAURON data, which does not vary down to R_e and, for simplicity, is represented as a single point at R= 50″. Information at higher radial distances, obtained from the literature, was added to have an overall picture of the whole galaxy. Green circles show the values of age and metallicity derived by Liu et al. (2005). The literature data are taken from several sources and different stellar population models or relationships (Pegase models from Fioc & Rocca-Volmerange 1997, 1999 for Liu et al. 2005; Schiavon 2007 models for Kuntschner et al. 2010; Casuso et al. 1996 relationship for Davies, Sadler & Peletier 1993; BC03 for this work). As the comparison among these different models is not straightforward, we do not consider a direct quantitative comparison in this work. In any case, trends and gradients can be compared qualitatively regardless of the absolute value.

Although the optical+NIR photometry allows us to reasonably disentangle age and metallicity (see Anders et al. 2004), we are not able to constrain both metallicity and [α/Fe] separately, and our metallicity profiles can indeed be affected by radial changes of [α/Fe]. However, it is worth noting that in Kuntschner et al. (2010) the values of [α/Fe] are 0.41$\pm$0.05 and 0.44$\pm$0.05 for apertures of radii R_e/8 and R_e, respectively, indicating almost no change within errors and supporting our interpretation that the results reflect a [Fe/H] gradient.

As seen in Figure 4, the age radial profile is compatible with no age variation down to M87's R_e ($\sim$ 8 kpc), although in the inner 20″ the area of the polygon is wide enough to contain ages down to 3 Gyr due to age-metallicity degeneracy. Kuntschner et al. (2010) data (represented by a red square, shifted to 14 Gyr) also agree with no age variation for M87 at these radii. Despite the large errors in our results, we can rule out young ages for large radii (where our photometrical errors are smaller) as the polygon tends to get narrower outwards, due to the smaller errors of SDSS photometry.

The metallicity profile presents a *plateau* for the inner 1 kpc, also observed in the flattening of the colour profiles (see Section 3.1). Still, super solar metallicity values are expected for the central 1 kpc while towards larger radii the metallicity seems to decrease, i.e., metallicity descend below solar abundance. Davies, Sadler & Peletier (1993) studied out to 50″ from the centre of M87 using absorption-line strengths in spectra (purple stars). Although our *plateau* could be argued to be a consequence of reaching the maximum metallicity provided in BC03 (see below), it is also observed in their data, as well as the decrease of the metallicity with radius. This strongly suggests that the inner plateau in the metallicity is real.

Kuntschner et al. (2010) using SAURON measured the properties of M87 using integral field spectroscopy (red squares). Their metallicity profile surprisingly resembles our profile too, although Kuntschner et al. (2010) absolute values in the central parts are lower. It also reproduces the *plateau* at R$<$ 10″. Their estimated ages ($\sim$ 17 Gyr) are rescaled according to the maximum age set in Section 3.2.1: 14 Gyr. Note that the H_β line-strengths are significantly and systematically weaker than the stellar population model

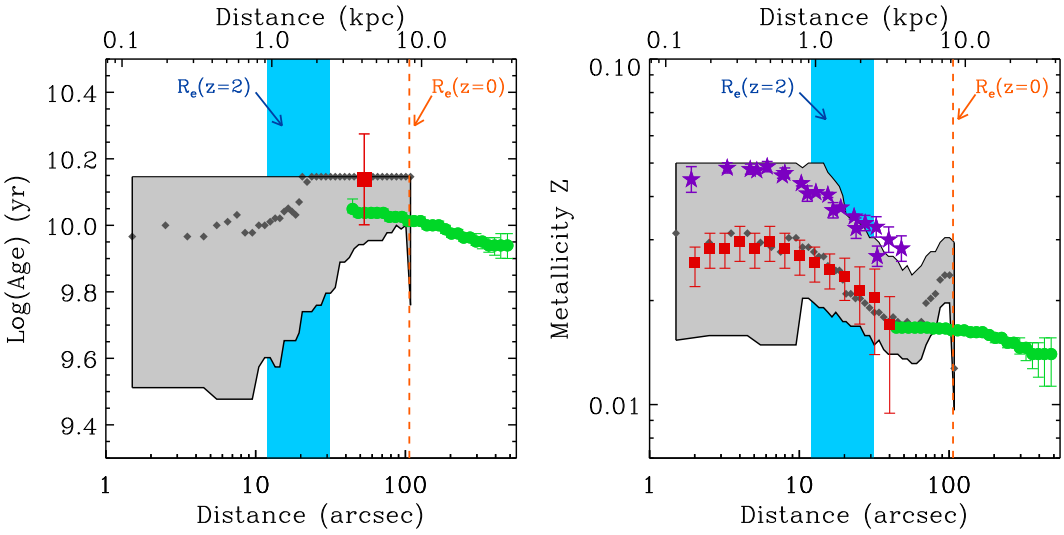

Figure 4. Gradients of age and metallicity with radial distance for M87. The grey polygon is the 68% confidence region resulting from the BC03 SSP model fit to our data and the dark grey diamonds represent the model with the minimum $\tilde{\chi}^2$. Red squares represent the data obtained with SAURON for the central region of M87 (Kuntschner et al. 2010). Green circles show the values of age and metallicity derived by Liu et al. (2005). Purple stars are data from Davies, Sadler & Peletier (1993) using absorption-line strength of Mg_2. We have shifted the age estimates of Kuntschner et al. (2010) from 17.7 Gyr to 14 Gyr. The orange dashed line indicates the position of M87's R_e. The blue polygon defines the range of possible values for the size of M87 at z= 2.

predictions (see Kuntschner et al. 2010) causing that the derived ages to saturate at the maximum allowed age of the models ($\sim$ 17 Gyr). Therefore we have to be cautious deriving conclusions using this profile. Assuming that no changes are made by the indetermination of ages, we can say there is an agreement between the metallicity profiles.

The gradient of the entire profile, calculated as a linear fit of the metallicity [Z/H] vs. $\log$ R is -0.26 ± 0.10 (-0.25 ± 0.09 for a Chabrier IMF). The Mg_2 data obtained by Davies, Sadler & Peletier (1993) also show a gradient in metallicity compatible with our results (-0.21 ± 0.01). They also find a slightly positive slope for the H_β profile.

Furthermore, we have also explored the metallicity profile imposing an age constraint, from 10 to 14 Gyr. It seems reasonable to assume old ages for the bulk of stars of the galaxy as seen in previous studies (e.g. Liu et al. 2005; Kuntschner et al. 2010). The results are presented in Figure C2. The main difference compared to Figure 4 is that the width of the allowed metallicity solutions has decreased in the range from 10″ to 20″. Consequently, this result supports the idea that the *plateau* is a real characteristic of the metallicity profile of M87 and not an artifact due to limitations of the models. In this case, the gradient is -0.27 ± 0.08.

Our results are complemented with photometric derived ages and metallicities from Liu et al. (2005) up to $5\,R_e$. Their ages are in agreement with our results in the overlapping region, as well as with our metallicities. The gradient in metallicity of Liu et al. (2005) is -0.080 ± 0.006, shallower than what it is found here. However, there is a hint in our data of a change in the slope of the profile towards 60 arcsec ($\sim$ 5 kpc) to a much shallower gradient, as observerd in Liu et al. (2005). This change in the slope may be originated by the evolution of the galaxy as we will discuss below. However, note that this change in our metallicity profile coincides with the change of behaviour in the $g - z$ colour (while the increase in the minimum $\tilde{\chi}^2$ in Figure C1 is due to the underestimation of the u and IR photometry), therefore the conclusions of our work are based in Liu et al. (2005) results.

4 DISCUSSION

Using HR photometry combined with wide field literature data, we have derived ages and metallicities for the inner R_e of M87 using SED fitting. We found that changes in metallicity can explain why colours become bluer towards the outer parts of the galaxy. The metallicity profile decreases with radius while ages are constant down to M87's R_e. The metallicity radial profile of M87 presents three different zones: in the innermost kpc a *plateau* with supersolar metallicity, a decline in metallicity down to $\sim$ 5 kpc which is followed by an almost flat region with near solar metallicity. The shape of the metallicity profile is independent of the IMF used, Salpeter or Chabrier, as shown in Appendix C. Down to the R_e of M87, the age of the stellar population is old ($>$ 10 Gyr) and the lack of an age gradient is compatible with a rapid episode of star formation in the past.

4.1 Comparison with previous studies

As mentioned before, our age and metallicity estimates are in agreement with previous determinations of these values by Kuntschner et al. (2010) and Liu et al. (2005). In addition, studies of globular clusters in M87 (e.g. Cohen, Blakeslee & Ryzhov 1998; Jordán et al. 2002) and their link to the galaxy itself (Kundu et al. 1999; Harris 2009) also support old ages for the bulk of stars of the galaxy,

similar to what we find in this work. Our metallicities are supersolar and show evidence for a gradient towards the outer parts of the galaxy as expected from its colour profiles (Section 3.1, and Peletier, Valentijn & Jameson 1990). This is also observed in Davies, Sadler & Peletier (1993); Liu et al. (2005) and in Kuntschner et al. (2010).

The age of the stellar population of M87 shows no variation in agreement with the lack of gradient found in massive ellipticals in, for example, Sánchez-Blázquez, Gorgas & Cardiel (2006); Sánchez-Blázquez et al. (2007); Spolaor et al. (2008, 2010); Kuntschner et al. (2010); Loubser & Sánchez-Blázquez (2012). It is worth noting however that, Davies, Sadler & Peletier (1993) find a slightly positive H_β gradient, but possibly related to contamination from H_β emission observed in this galaxy. Conversely, Liu et al. (2005) found a mild decrease in age for the outer parts of the galaxy ($R \gtrsim R_e/2$) compatible with some galaxies in Greene et al. (2012) but contrary to the results found in Sánchez-Blázquez et al. (2007); La Barbera et al. (2010, 2012) where null or positive age gradients are observed in early-type galaxies.

Our global metallicity gradient is -0.26 ± 0.10. Similarly, Davies, Sadler & Peletier (1993) found a metallicity gradient of -0.21 ± 0.01 using absorption-line measurements of Mg_2 of the central part of M87 up to $\sim 50''$. As we show now, gradients obtained in other galaxies are similar. The mean metallicity gradient of Kuntschner et al. (2010) sample of old galaxies (> 8 Gyr) is -0.25 ± 0.11. For Loubser & Sánchez-Blázquez (2012) sample of bright cluster galaxies, the metallicity gradient is -0.29 ± 0.06 and for galaxies in the Coma cluster of Sánchez-Blázquez, Gorgas & Cardiel (2006) is -0.33 ± 0.16. However, for $R > R_e$ the gradient turns into -0.080 ± 0.006 for M87 (Liu et al. 2005), compatible with the gradients of low-mass early-type galaxies (Spolaor et al. 2009).

In relation to the different gradients observed in the metallicity profile, NGC 4889, one of the two central bright cluster galaxies of the Coma cluster show comparable gradients to M87's (Coccato, Gerhard & Arnaboldi 2010). Two different metallicity gradients are observed for the inner part ($R \lesssim 1.2R_e$; -0.35 ± 0.02) and outer part ($R \gtrsim 1.2R_e$; -0.1 ± 0.2). Moreover, Baes et al. (2007) find a also a break in the slopes of the metallicity gradients, getting shallower at larger radii. A similar change in gradient for a radius $\sim R_e$ is observed in our results. This potentially indicates that different mechanisms formed the central parts of the galaxy and the outer regions.

Summarizing, the results found in our work are similar to those found by other authors in M87 and in other massive early-type galaxies. It is worth noting that the results for M87 might be generalized only to the case of galaxies being the central objects in dark matter halos, and not massive galaxies as a whole, as central galaxies are observed to have different properties than satellites (e.g. Pasquali et al. 2010).

4.2 How can M87's age and metallicity profiles help us to understand its formation?

According to the current scenario of galaxy formation and evolution, massive galaxies were assembled in two different phases (e.g. Naab, Johansson & Ostriker 2009). In the first phase, the innermost regions formed the majority of their stars at high redshift and on short timescales (e.g. Thomas et al. 2005). During this dissipative "monolithic collapse", stars were efficiently created while the gas sank to the centre of the forming galaxy. As a consequence of this process, a negative radial metallicity gradient was created with the central stars being more metal-rich than the stars in the outskirts. For example, Larson (1974) estimated a metallicity gradient of ~ -0.35, ~ -0.5 for Carlberg (1984) and -1.0 in Kobayashi (2004). However, the rapid formation of the galaxy produced almost no noticeable variation in age.

In the second phase of the galaxy formation, there is a size growth of the galaxies driven by the accretion of low-mass satellites. These satellites, mostly depleted of gas, end located in the outskirts of these galaxies (e.g. Khochfar & Silk 2006). For this reason, one would expect a significant change in the stellar properties with radius as the stars of these merged satellites are mainly located in the periphery of the main galaxy due to their higher angular momentum. These stars should be relatively evolved and no star formation is expected to occur if mergers are dry. Consequently, the new accreted stars are not expected to produce significant age variations in the galaxy. As the stars of these low-mass satellites will be metal-poor (as indicated by observations, e.g. Spolaor et al. 2009), the radial metallicity gradient is predicted to change due to the contribution of metal-poor stars from the shreded satellites (Naab, Johansson & Ostriker 2009). For instance, one could expect a steepening of the metallicity gradient in the outskirts. In other words, we expect a steep negative radial gradient in the inner region of the galaxy while in the outer parts a change of gradient is suggested. On what follows, we discuss how our results fit in this picture.

One of the most intriguing results that we have found in this paper is the presence of a *plateau* in the colour profiles and in the metallicity gradient of M87 at $R \lesssim 1$ kpc. This flattening in the metallicity profile is not expected in the models of a dissipative "monolithic collapse". Is this *plateau* a real property of the metallicity profile? As shown in Figure 4, Davies, Sadler & Peletier (1993) and Kuntschner et al. (2010) found the same behaviour using ground-based data affected by seeing up to $3''$ and $1''$, respectively. Our HR results, show that the metallicity flattening is not caused by the blurring effect of their seeing. Intriguingly, this inner *plateau* is not a unique feature of M87. In fact, this kind of behaviour is also observed in Sánchez-Blázquez et al. (2007), where a similar flattening for the inner $\sim 9''$ (~ 2.5 kpc) is present in the metallicity profile of the field massive galaxy NGC 1600.

How can we explain this metallicity *plateau* (~ 1 kpc) in the context of massive galaxy formation? The timescales for dissipative collapse are of $< 0.5 - 1$ Gyr (Pipino, D'Ercole & Matteucci 2008). To explore the feasibility of these short timescales for the formation of the innermost region of M87, we have estimated the mass enclosed by the *plateau* using Equation 15 in Trujillo, Graham & Caon (2001). Almost 10% of the mass of M87 is within ~ 1 kpc. That is $\sim 7 \times 10^{10}\, M_\odot$, assuming that the total stellar mass of M87 is $6.8 \pm 1.1 \times 10^{11}\, M_\odot$ (taken from Forte, Vega & Faifer 2012). So, the star formation rate within ~ 1 kpc should have been $\gtrsim 70 - 140\, M_\odot\, yr^{-1}$. Star

formation rates as high as $\sim 3000\,\mathrm{M}_\odot\,\mathrm{yr}^{-1}$ have been found in a massive starbursts galaxies at $z \sim 6$ (Riechers et al. 2013). Consequently, a rapid monolithic collapse looks like a very plausible scenario. New evidence in the recently discovered relic galaxy NGC 1277 (Trujillo et al. 2013) also support this picture.

Moreover, the size of this *plateau* can provide clues about the size evolution of M87. It is widely known that high-redshift massive galaxies were smaller in size than their present-day massive counterparts (e.g. Daddi et al. 2005; Trujillo et al. 2006; Buitrago et al. 2008). Possibly, this evolution in size has left a signature on the properties of the stellar populations of M87. For this reason, we have calculated the R_e that a galaxy like M87 would have had at $z = 2$. Using the following equation for size evolution (in Trujillo, Ferreras & de La Rosa 2011):

$$\log R_f = \log R_i + \Delta \log R|_{M_{i,fixed}} + C \log(M_f/M_i) \qquad (3)$$

where R_f and M_f are the radius and the mass at $z = 0$, and R_i and M_i the radius and the mass at a given z. $\Delta \log R|_{M_{i,fixed}}$ accounts for the variation of the radius at a fixed mass, while the term $C \log(M_f/M_i)$ reflects the change in radius due to the variation of the mass as a consequence of the accretion of satellite galaxies. Many of the previous parameters are fixed by the observations. For instance, we know that galaxies have doubled their mass since $z = 2$ (van Dokkum et al. 2010), $C = 0.56$ from Shen et al. (2003) and the evolution in radius at a fixed stellar mass is described by $R_i = R_f(1 + z)^\beta$. The β parameter ranges from -0.75 to -1.62 (see Oser et al. 2012, and references therein). We assume that R_f is the observed R_e of M87 at $z = 0$ ($106\farcs2$, Falcón-Barroso et al. 2011). The above values provide us with a region of potential values for the size (R_e) of M87 at $z = 2$. We obtain that M87 R_e at $z = 2$ should have been between 0.94 kpc to 2.5 kpc in agreement with the position of the turning point of the *plateau* at ~ 1 kpc, given that the formation of this flattening was occured very early-on. This region is shaded in light blue in Figure 4. As discussed in Falcón-Barroso et al. (2011), the value of the R_e of M87 is uncertain. According to the size distribution of galaxies in Shen et al. (2003), we expect a higher R_e (~ 10 kpc). Therefore, the values obtained for the size of M87 at z~ 2 could range between 1 kpc and 3 kpc, still compatible with our results. This matches the picture that this flattening of the metallicity provides a signature of the size of the proto-galaxy at $z = 2$, after its quick formation.

Concerning the rest of the galaxy, beyond the inner *plateau* there is a zone of declining metallicity observed from $\sim$ 1 kpc to $\sim$ 5 kpc (see Figure 4). Although the global gradient is -0.26 ± 0.10, the local gradient for this region, between 1 to 5 kpc, is steeper:-0.4 ± 0.2. This steep metallicity gradient down to R_e is reminiscent of the predictions of the dissipative quasi-monolithic collapse mentioned before (e.g. Larson 1974; Carlberg 1984; Kobayashi 2004; Pipino, D'Ercole & Matteucci 2008). The slopes range between ~ -1 to ~ -0.35 for different models, in agreement with the gradient found in M87. While this dissipative process tend to create metallicity gradients, mergers between galaxies destroy these gradients (e.g. White 1980; Kobayashi 2004). Our derived metallicity gradient is compatible with the ~ -0.3 for galaxies built in a dissipative collapse. Consequently, the observed [Z/H] gradient is probably the consequence of the dissipative formation of this zone of the galaxy. In short, the inner 5 kpc of M87 seems to have formed through a dissipative collapse, with the innermost 1 kpc having formed in a extremely short timescale as suggested by the *plateau* in its metallicity gradient.

Outwards, at $\gtrsim$ 5 kpc, there is a change in the metallicity gradient that becomes flat at these distances. This evidence of a change of slope supports the scenario, as discussed above, where the centre of the galaxy formed via a rapid dissipative process whereas the rest of the galaxy was built via accretion of low-mass satellites. If these low-mass systems had been accreted in a more massive galaxy, different gradients are a natural outcome as the stars tend to populate the outer parts of the galaxy as seen in, for example, Coccato, Gerhard & Arnaboldi (2010). This flattening suggests that most of the mass that built the outskirsts of the galaxy came from satellites of similar metallicity (subsolar). Moreover, this gradient turning point denotes where the influence of the massive proto-galaxy ends (i.e. at $2-3\,R_e$ at $z = 2$).

This behaviour of the metallicity gradient is consistent with recent studies (e.g. Daddi et al. 2005; Trujillo et al. 2006; Trujillo, Ferreras & de La Rosa 2011) where early-type galaxies have sizes a factor of 4 larger than their counterparts at $z \sim 2$. The central stellar mass density of the massive galaxies at high-z do not differ much from the central density of nearby galaxies (Hopkins et al. 2009). Consequently the majority of the evolution has taken place in their outer regions. The high dispersion in gradients for high-mass galaxies observed in Spolaor et al. (2009) also points to minor mergers as a mechanism for the build-up of the galaxy.

In summary, the metallicity profile presents three different zones that correspond to two separate mechanisms for the formation of the galaxy. The inner parts of the galaxy, R$\lesssim$ 5 kpc, are likely formed as a result of a dissipative event in the past. They have formed very rapidly, especially the very central $\sim$ 1 kpc which seems to be the consequence of a very intense burst of star formation. Oppositely, the outer galaxy, R$\gtrsim$ 5 kpc may be the result of the accretion of low-mass galaxies.

5 SUMMARY AND CONCLUSIONS

Using HR imaging from *HST* and adaptive optics from NaCo at VLT, we derived radial SEDs for the central $\sim$ 1 kpc of M87. This dataset was complemented with wide field imaging from GALEX, SDSS and 2MASS to reach up to M87's R_e ($\sim$ 8 kpc). Constructing colours from this dataset, radial changes in the stellar populations are seen. Studying this in more detail through SED fitting, we found that radial variations trace changes in metallicity (Section 3.2). Adding data from the literature up to $5R_e$, three different behaviours for the metallicity profile are observed: a central flattening or *plateau* at R$\lesssim$ 1 kpc, a decline in metallicity down to R_e and a change in the metallicity gradient for R$>$ R_e. The central metallicity gradient agrees with previous estimates of M87 with absorption line strengths. The metallicity structure of M87 is consistent with the current scenario of galaxy formation where the central part of the galaxy had formed first and the outer part was accreted via dry minor merging.

ACKNOWLEDGEMENTS

We thank the anonymous referee for his/her detailed and constructive comments that improved the paper. We also thank A. Vazdekis and P. Sánchez-Blázquez for many useful comments on stellar population gradients, H. Kuntschner for kindly providing the SAURON metallicity profile of M87 and A. Gil de Paz, C.-W. Chen and R. Läsker for providing the GALEX, SDSS and K radial profiles of M87, respectively. This work is partially funded by the Spanish MEC project AYA2007-60235 and AYA2010-21322-C03-02.

REFERENCES

Anders P., Bissantz N., Fritze-v. Alvensleben U., de Grijs R., 2004, MNRAS, 347, 196
Baes M. et al., 2010, A&A, 518, L53
Baes M., Sil'chenko O. K., Moiseev A. V., Manakova E. A., 2007, A&A, 467, 991
Bertin E., Arnouts S., 1996, A&AS, 117, 393
Blakeslee J. P., Lucey J. R., Barris B. J., Hudson M. J., Tonry J. L., 2001, MNRAS, 327, 1004
Bruzual G., Charlot S., 2003, MNRAS, 344, 1000
Buitrago F., Trujillo I., Conselice C. J., Bouwens R. J., Dickinson M., Yan H., 2008, ApJ, 687, L61
Cardelli J. A., Clayton G. C., Mathis J. S., 1989, ApJ, 345, 245
Carlberg R. G., 1984, ApJ, 286, 416
Casuso E., Vazdekis A., Peletier R. F., Beckman J. E., 1996, ApJ, 458, 533
Cenarro A. J., Gorgas J., Vazdekis A., Cardiel N., Peletier R. F., 2003, MNRAS, 339, L12
Chabrier G., 2003, ApJ, 586, L133
Chen C.-W., Côté P., West A. A., Peng E. W., Ferrarese L., 2010, ApJS, 191, 1
Chiosi C., Carraro G., 2002, MNRAS, 335, 335
Coccato L., Gerhard O., Arnaboldi M., 2010, MNRAS, 407, L26
Cohen J. G., 1986, AJ, 92, 1039
Cohen J. G., Blakeslee J. P., Ryzhov A., 1998, ApJ, 496, 808
Corbin M. R., O'Neil E., Rieke M. J., 2002, AJ, 124, 183
Daddi E. et al., 2005, ApJ, 626, 680
Davies R. L., Sadler E. M., Peletier R. F., 1993, MNRAS, 262, 650
de Vaucouleurs G., Nieto J.-L., 1978, ApJ, 220, 449
Dorman B., O'Connell R. W., Rood R. T., 1995, ApJ, 442, 105
Eggen O. J., Lynden-Bell D., Sandage A. R., 1962, ApJ, 136, 748
Falcón-Barroso J. et al., 2011, MNRAS, 417, 1787
Ferreras I., La Barbera F., de la Rosa I. G., Vazdekis A., de Carvalho R. R., Falcón-Barroso J., Ricciardelli E., 2013, MNRAS, 429, L15
Fioc M., Rocca-Volmerange B., 1997, A&A, 326, 950
—, 1999, ArXiv Astrophysics e-prints
Ford H. C. et al., 1994, ApJ, 435, L27
Forte J. C., Vega E. I., Faifer F., 2012, MNRAS, 421, 635
Franx M., Illingworth G., 1990, ApJ, 359, L41
Fruchter A. S., Hook R. N., 2002, PASP, 114, 144
Gil de Paz A. et al., 2007, ApJS, 173, 185
Greene J. E., Murphy J. D., Comerford J. M., Gebhardt K., Adams J. J., 2012, ApJ, 750, 32
Harris W. E., 2009, ApJ, 703, 939
Hopkins P. F., Bundy K., Murray N., Quataert E., Lauer T. R., Ma C.-P., 2009, MNRAS, 398, 898
Jarrett T. H., Chester T., Cutri R., Schneider S. E., Huchra J. P., 2003, AJ, 125, 525
Jordán A., Côté P., West M. J., Marzke R. O., 2002, ApJ, 576, L113
Khochfar S., Silk J., 2006, MNRAS, 370, 902
Kissler-Patig M., Brodie J. P., Minniti D., 2002, A&A, 391, 441
Kobayashi C., 2004, MNRAS, 347, 740
Kundu A., Whitmore B. C., Sparks W. B., Macchetto F. D., Zepf S. E., Ashman K. M., 1999, ApJ, 513, 733
Kuntschner H. et al., 2010, MNRAS, 408, 97
La Barbera F., De Carvalho R. R., De La Rosa I. G., Gal R. R., Swindle R., Lopes P. A. A., 2010, AJ, 140, 1528
La Barbera F., Ferreras I., de Carvalho R. R., Bruzual G., Charlot S., Pasquali A., Merlin E., 2012, MNRAS, 426, 2300
Larson R. B., 1974, MNRAS, 166, 585
Läsker R., Ferrarese L., van de Ven G., 2013, ArXiv e-prints:1311.1530
Liu Y., Zhou X., Ma J., Wu H., Yang Y., Li J., Chen J., 2005, AJ, 129, 2628
Loubser S. I., Sánchez-Blázquez P., 2012, MNRAS, 425, 841
Merlin E., Chiosi C., Piovan L., Grassi T., Buonomo U., Barbera F. L., 2012, MNRAS, 427, 1530
Naab T., Johansson P. H., Ostriker J. P., 2009, ApJ, 699, L178
O'Connell R. W., 1999, ARA&A, 37, 603
Ogando R. L. C., Maia M. A. G., Chiappini C., Pellegrini P. S., Schiavon R. P., da Costa L. N., 2005, ApJ, 632, L61
Ohl R. G. et al., 1998, ApJ, 505, L11
Oser L., Naab T., Ostriker J. P., Johansson P. H., 2012, ApJ, 744, 63
Pasquali A., Gallazzi A., Fontanot F., van den Bosch F. C., De Lucia G., Mo H. J., Yang X., 2010, MNRAS, 407, 937
Peletier R. F., 1989, PhD thesis, , University of Groningen, The Netherlands, (1989)
Peletier R. F., Valentijn E. A., Jameson R. F., 1990, A&A, 233, 62
Pipino A., D'Ercole A., Chiappini C., Matteucci F., 2010, MNRAS, 407, 1347
Pipino A., D'Ercole A., Matteucci F., 2008, A&A, 484, 679
Planck Collaboration et al., 2013, ArXiv e-prints, arXiv:1303.5076
Pogge R. W., Maoz D., Ho L. C., Eracleous M., 2000, ApJ, 532, 323
Riechers D. A. et al., 2013, Nature, 496, 329
Roediger J. C., Courteau S., MacArthur L. A., McDonald M., 2011, MNRAS, 416, 1996
Salpeter E. E., 1955, ApJ, 121, 161
Sánchez-Blázquez P., Forbes D. A., Strader J., Brodie J., Proctor R., 2007, MNRAS, 377, 759
Sánchez-Blázquez P., Gorgas J., Cardiel N., 2006, A&A, 457, 823
Schiavon R. P., 2007, ApJS, 171, 146
Schlegel D. J., Finkbeiner D. P., Davis M., 1998, ApJ, 500, 525

Sérsic J. L., 1968, Atlas de galaxias australes
Shen S., Mo H. J., White S. D. M., Blanton M. R., Kauffmann G., Voges W., Brinkmann J., Csabai I., 2003, MNRAS, 343, 978
Skrutskie M. F. et al., 2006, AJ, 131, 1163
Sohn S. T., O'Connell R. W., Kundu A., Landsman W. B., Burstein D., Bohlin R. C., Frogel J. A., Rose J. A., 2006, AJ, 131, 866
Spolaor M., Forbes D. A., Proctor R. N., Hau G. K. T., Brough S., 2008, MNRAS, 385, 675
Spolaor M., Kobayashi C., Forbes D. A., Couch W. J., Hau G. K. T., 2010, MNRAS, 408, 272
Spolaor M., Proctor R. N., Forbes D. A., Couch W. J., 2009, ApJ, 691, L138
Tal T., van Dokkum P. G., 2011, ApJ, 731, 89
Thomas D., Maraston C., Bender R., Mendes de Oliveira C., 2005, ApJ, 621, 673
Trujillo I., Ferre-Mateu A., Balcells M., Vazdekis A., Sanchez-Blazquez P., 2013, ArXiv e-prints
Trujillo I., Ferreras I., de La Rosa I. G., 2011, MNRAS, 415, 3903
Trujillo I. et al., 2006, ApJ, 650, 18
Trujillo I., Graham A. W., Caon N., 2001, MNRAS, 326, 869
van Dokkum P. G., Conroy C., 2010, Nature, 468, 940
van Dokkum P. G. et al., 2010, ApJ, 709, 1018
White S. D. M., 1980, MNRAS, 191, 1P
York D. G. et al., 2000, AJ, 120, 1579
Zibetti S., Gallazzi A., Charlot S., Pierini D., Pasquali A., 2013, MNRAS, 428, 1479

This paper has been typeset from a TEX/ LATEX file prepared by the author.

APPENDIX A: THE RADIAL PROFILES OF THE CENTRE OF M87

Here we present the photometric data derived for the centre of M87 using HR imaging. The photometric errors are derived from the residuals to Sérsic fits as explained in Section 2.2.4. The quality of STIS F25QTZ image (NUV) just allows us to derive reliable photometry up to R= 5.5″.

Table A1: Data for the inner 19″ of M87

Radius (″)	FUV	NUV	F336W	F410M	F467M	F475W	F555W	F547M	F606W	F658N	F702W	F814W	F850LP	J	F160W	K_s
	[mag/arcsec^2]															
1.5	21.93	21.66	19.76	18.50	17.67	17.63	17.15	17.03	16.85	16.45	16.48	16.18	15.97	15.61	15.33	15.54
2.5	22.15	21.96	19.94	18.64	17.81	17.77	17.30	17.17	17.00	16.67	16.64	16.33	16.11	15.74	15.48	15.69
3.5	22.32	22.16	20.07	18.76	17.93	17.89	17.41	17.29	17.13	16.86	16.76	16.45	16.24	15.86	15.61	15.82
4.5	22.47	22.34	20.19	18.87	18.05	18.00	17.53	17.40	17.25	17.00	16.88	16.57	16.35	15.97	15.72	15.94
5.5	22.60	22.53	20.31	18.98	18.16	18.12	17.65	17.52	17.37	17.12	17.00	16.69	16.48	16.08	15.84	16.06
6.5	22.75	...	20.43	19.10	18.29	18.24	17.77	17.64	17.49	17.25	17.12	16.81	16.60	16.20	15.96	16.18
7.5	22.89	...	20.55	19.23	18.41	18.37	17.89	17.77	17.62	17.37	17.25	16.94	16.72	16.31	16.08	16.30
8.5	22.99	...	20.68	19.35	18.54	18.49	18.01	17.89	17.74	17.50	17.37	17.07	16.85	16.42	16.20	16.43
9.5	23.14	...	20.80	19.47	18.66	18.61	18.13	18.02	17.86	17.62	17.49	17.19	16.97	16.52	16.32	16.55
10.5	23.25	...	20.93	19.59	18.78	18.73	18.25	18.14	17.98	17.75	17.62	17.31	17.09	...	...	...
11.5	23.36	...	21.05	19.70	18.90	18.84	18.37	18.26	18.10	17.86	17.74	17.43	17.21	...	...	...
12.5	23.44	...	21.17	19.81	19.02	18.95	18.48	18.38	18.21	17.97	17.85	17.54	17.32	...	...	...
13.5	23.54	...	21.29	19.92	19.13	19.06	18.59	18.49	18.32	18.08	17.96	17.65	17.43	...	...	...
14.5	23.62	...	21.40	20.02	19.24	19.16	18.69	18.59	18.42	18.19	18.07	17.75	17.53	...	...	...
15.5	23.71	...	21.50	20.11	19.35	19.25	18.79	18.69	18.52	18.30	18.17	17.85	17.63	...	...	...
16.5	23.78	...	21.57	20.21	19.43	19.35	18.89	18.78	18.61	18.40	18.27	17.94	17.73	...	...	...
17.5	23.85	...	21.64	20.30	19.51	19.43	18.99	18.87	18.70	18.49	18.37	18.04	17.82	...	...	...

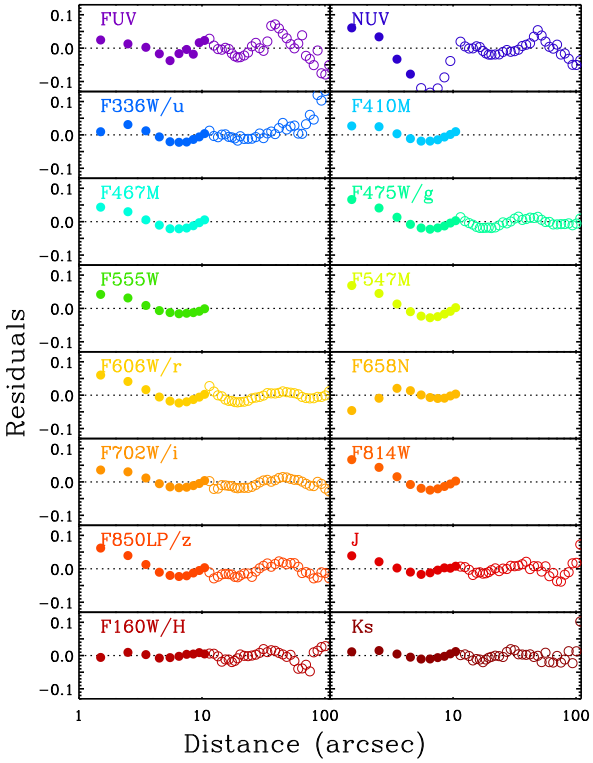

Figure B1. Residuals of the observed profiles after substracting their corresponding Sérsic fits. The filled circles indicate HR profiles while the open circles depict the wide-fiel data.

Filter	Shift	r.m.s
	[mag/arcsec^2]	
FUV STIS	-0.21	0.096
NUV STIS	0.50	
F336W	-0.25	0.050
F410M	-0.02	0.020
F467M	-0.02	0.010
F475W	-0.04	0.006
F555W	-0.10	0.010
F547M	-0.40	0.030
F606W	-0.11	0.007
F702W	-0.15	0.014
F814W	-0.10	0.009
F850LP	-0.10	0.015
J NaCo	0.08	0.014
F160W	-0.01	0.005
K NaCo	0.0	0.010

Table B1. Offset and r.m.s between HR and wide-field profiles.

APPENDIX B: SÉRSIC FITS RESIDUALS AND HR/WIDE-FIELD OFFSETS

To illustrate how the errors have been estimated, we provide the residuals of the profiles to the corresponding Sérsic fits for HR and wide-field data in Figure B1. In Table B1, we also reported the shifts and the root mean square (r.m.s) between HR and wide-field profiles in the overlapping region.

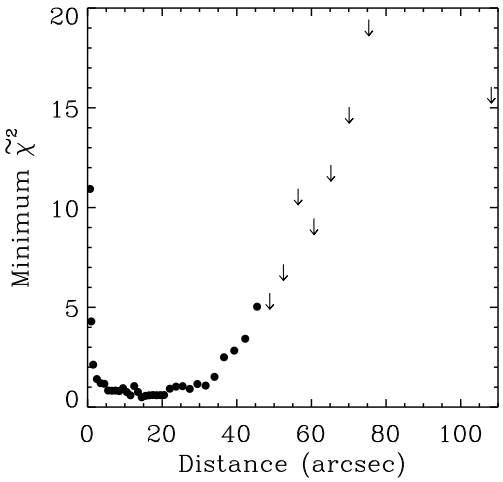

Figure C1. Minimum $\tilde{\chi}^2$ as a function of radius. It is clearly seen the effect of the incorrect sky substraction for u and 2MASS photometry at R$>40''$.

APPENDIX C: AGE AND METALLICITY RADIAL PROFILES FOR DIFFERENT CONSTRAINTS

Here we present the results of the fits to the radial SEDs of M87, following Section 3.2. Figure C1 shows the minimum $\tilde{\chi}^2$ as a function of radius corresponding to Figure 4. When the model is a good representation of the data and the errors are properly estimated, the expected values of $\tilde{\chi}^2$ should be around 1. For R$\gtrsim 40''$, the increase in the value of the $\tilde{\chi}^2$ is due to the effect of the sky oversubstraction in the 2MASS and u profiles. For this reason, the values are marked as upper limits.

We have also tested different SSPs contraints and models to check the reliability of our results. First, we imposed an age constraint: from 10 to 14 Gyr. It seems reasonable to assume an old age for the bulk of stars of the galaxy given the results of previous studies (e.g. Liu et al. 2005; Kuntschner et al. 2010). The results are presented in Figure C2. The uncertainty on the metallicity profile has decreased in the inner $20''$, not reaching the highest metallicity available for the models. Consequently, this result supports the idea that the *plateau* at R<1 kpc is a real characteristic of the metallicity profile of M87 and not an artifact due to the limitations of the models. We also present the results of using: BC03 models with a Chabrier (2003) in Figure C3 and Charlot & Bruzual (2007, priv. comm.) in Figure C4. The gradients are: -0.27 ± 0.08, -0.25 ± 0.09 and -0.29 ± 0.09, respectively.

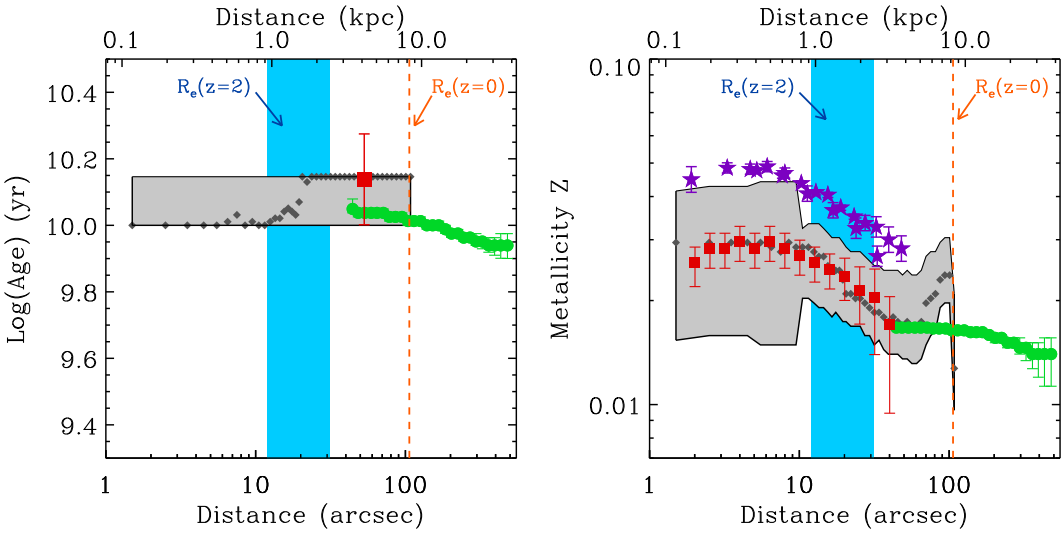

Figure C2. The same as in Figure 4 but using the BC03 SSP models with ages constrained from 10 to 14 Gyr. The gradient is: -0.27 ± 0.08.

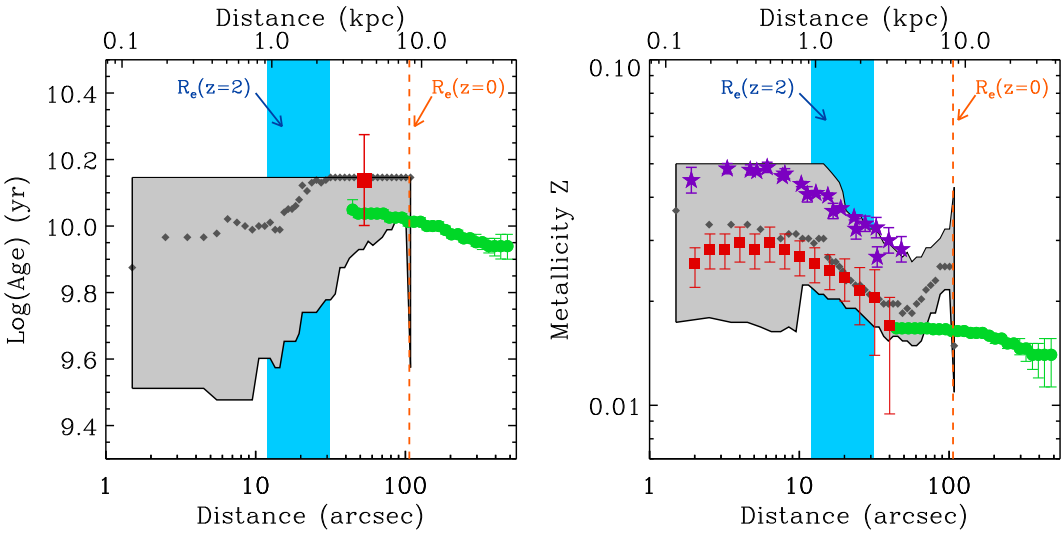

Figure C3. The same as in Figure 4 but using the BC03 SSP model with a Chabrier (2003) IMF. The gradient is: -0.25 ± 0.09.

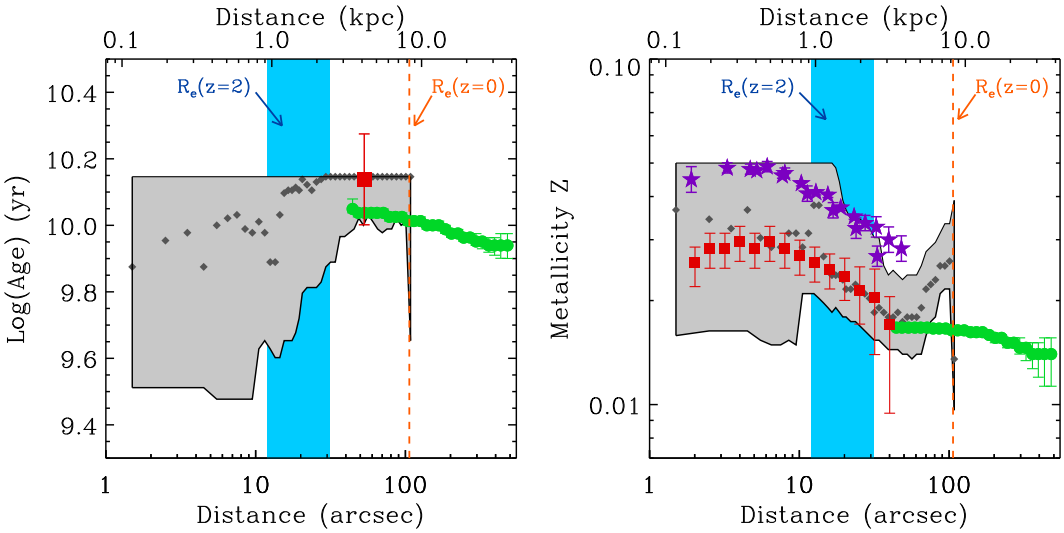

Figure C4. The same as in Figure 4 but using the Charlot & Bruzual (2007, in prep.) models. The gradient in this case is: -0.29 ± 0.09.